Lab on a Chip

PAPER

View Article Online
View Journal | View Issue

Cite this: *Lab Chip*, 2015, **15**, 1515

Ship-in-a-bottle femtosecond laser integration of optofluidic microlens arrays with center-pass units enabling coupling-free parallel cell counting with a 100% success rate†

Dong Wu,*[a] Li-Gang Niu,[b] Si-Zhu Wu,[a] Jian Xu,[a] Katsumi Midorikawa[a] and Koji Sugioka*[a]

Received 8th December 2014,
Accepted 15th January 2015

DOI: 10.1039/c4lc01439a

www.rsc.org/loc

Optimal design and fabrication of novel devices for high-performance optofluidic applications is a key issue for the development of advanced lab-on-a-chip systems. Parallel cell counting with a high success rate and simple mode of operation is a challenging goal. Current cell-counting methods, using optical waveguides or flow cytometry, typically require a precise coupling of the probe light and involve complex operations. In the present paper, a novel multifunctional cell counting microdevice is designed. It uses a center-pass optofluidic microlens array (MLA) consisting of seven microlenses and an M-shaped confining wall with 9 μm-diameter apertures. The device can be fabricated in a three-dimensional microchannel by ship-in-a-bottle femtosecond laser integration based on two-photon polymerization with optimized experimental parameters. Each microlens produces approximately the same intensity at the focal positions (within ±5%) under white-light illumination, while the confining wall restricts 6~8 μm-width cells to passing through the edges of two adjacent microlenses because the aperture opens toward their centers. The device demonstrates coupling-free parallel cell counting with a 100% success rate by monitoring the optical intensity variations at each spot. As a result, this method features both easy operation and high performance. Furthermore, the confining wall can filter deformed cells having 15 μm width.

1. Introduction

Over the past decade, microchips involving microfluidics,[1–3] optofluidics,[4–6] lab-on-a-chip devices,[7–9] and micro-total-analysis systems[10] have revolutionized chemical and biological studies by enabling reaction, detection, analysis, separation, and synthesis of materials with high efficiency, speed, and sensitivity at low reagent consumption and waste production.[11–13] One important biochip application is biological cell counting for cell-based life science research and medical inspections. Flow cytometry is the conventional method used to detect cells at low cost, but it requires high-power lasers and complex optomechanical systems.[14,15] To miniaturize and simplify cell detection, a variety of optofluidic devices have been developed, such as doped silicon dioxide waveguides connected to silicon microchannels,[16] pre-etched optical fibers inserted in glass microfluidic devices,[17,18] and SU-8 waveguides coupled with polymer microchannels.[19] To further simplify the fabrication process, many groups have proposed maskless femtosecond (fs) laser processing[20–28] to directly write optical waveguides[29–31] in transparent materials. The high peak intensity of a fs laser induces multiphoton absorption at the focal spot, enabling localized modifications of the refractive index in three dimensions. The pioneering report was that by Grigoropoulos *et al.* who reported cell detection using optofluidics fabricated by fs laser writing.[29] Their microfluidic channel was initially created in fused silica by fs laser-assisted wet etching (FLAE) which involves a laser direct-write modification followed by wet chemical etching. Next, the written optical waveguides were integrated with a three-dimensional (3D) glass microchannel. In another application, Bellouard *et al.* used optofluidics fabricated by the same technique with a four-quadrant photodetector to classify five algae species with an average positive identification rate of 78%.[30] However, these optical waveguides needed complex laser coupling systems and could only perform serial detection. Recently, integration of a microoptical component has been demonstrated using an array of high-performance

[a] *Laser Technology Laboratory, RIKEN, 2-1 Hirosawa, Wako, Saitama 351-0198, Japan. E-mail: ksugioka@riken.jp; Fax: +048 462 4682; Tel: +048 467 9492*
[b] *State Key Laboratory on Integrated Optoelectronics, College of Electronic Science and Engineering, Jilin University, 2699 Qianjin Street, Changchun, 130012, People's Republic of China*

† Electronic supplementary information (ESI) available. See DOI: 10.1039/c4lc01439a

polymer microlenses[32] created by fs two-photon polymerization (TPP).[33–38] This technique is termed ship-in-a-bottle integration, since the polymer microcomponents are created directly inside a hollow glass structure. The device successfully detected and counted cells with a 93% success rate under coupling-free white-light illumination.

Here, to further improve the success rate, a novel device is proposed based on a center-pass combined optofluidic MLA consisting of seven microlenses and an M-shaped confining wall having 9 μm-diameter apertures. The flexibility of ship-in-a-bottle integration enables fabrication of such a complex multifunctional device. Apertures in the confining wall open toward the center of each microlens so that the cells first pass through an aperture and then are guided to the space above the central position of the corresponding microlens. As a result, all cells passing through the confining wall can be detected to achieve a 100% counting rate. In addition to the coupling-free sensing, another feature of the device is its capability for parallel sensing based on the MLA, which can enhance the sensing speed. To optimize the design of the polymer microcomponents and the TPP experimental parameters, the polymer device is first fabricated on a flat glass surface and then integrated into a glass microchannel. Its 3D morphology, optical functions, and biological applications are systematically investigated using high-resolution scanning electron microscopy (SEM), transmission optical microscopy, and home-made characterization systems.

2. Experimental

Design and fabrication of a center-pass combined optofluidic lens array

A 522 nm fs laser beam generated from the second harmonic of an amplified Yb-doped fiber laser (FCPA μJewel D-400 from IMRA America having a wavelength of 1045 nm, a pulse width of 360 fs, and a repetition rate of 200 kHz) is used for both the FLAE and TPP processes, as shown in Fig. 1(a) and (b). Three-dimensional smooth microchannels are created by FLAE using commercial photosensitive Foturan glass (from Schott Glass) in a four-step procedure. First, a fs laser is used with a 20× objective lens having a numerical aperture of 0.46 to write 3D latent images inside the glass. Next, an initial anneal serves to develop the modified regions. Third, HF etching selectively removes the modified regions. Finally, another anneal is used to smooth the etched surfaces. The details of the procedure and experimental conditions have been previously reported.[26,39] The resulting glass microchannel is filled with the commercial epoxy-based negative-type resin SU-8 (2075 from MicroChem) for ship-in-a-bottle integration based on TPP. During the TPP laser writing (at 100 μW), an oil immersion 100× objective lens with a high numerical aperture of 1.4 is used for high-precision microfabrication. After successive processes of prebaking, laser direct writing, postbaking, and development, the 3D polymer microlens array is integrated into the glass

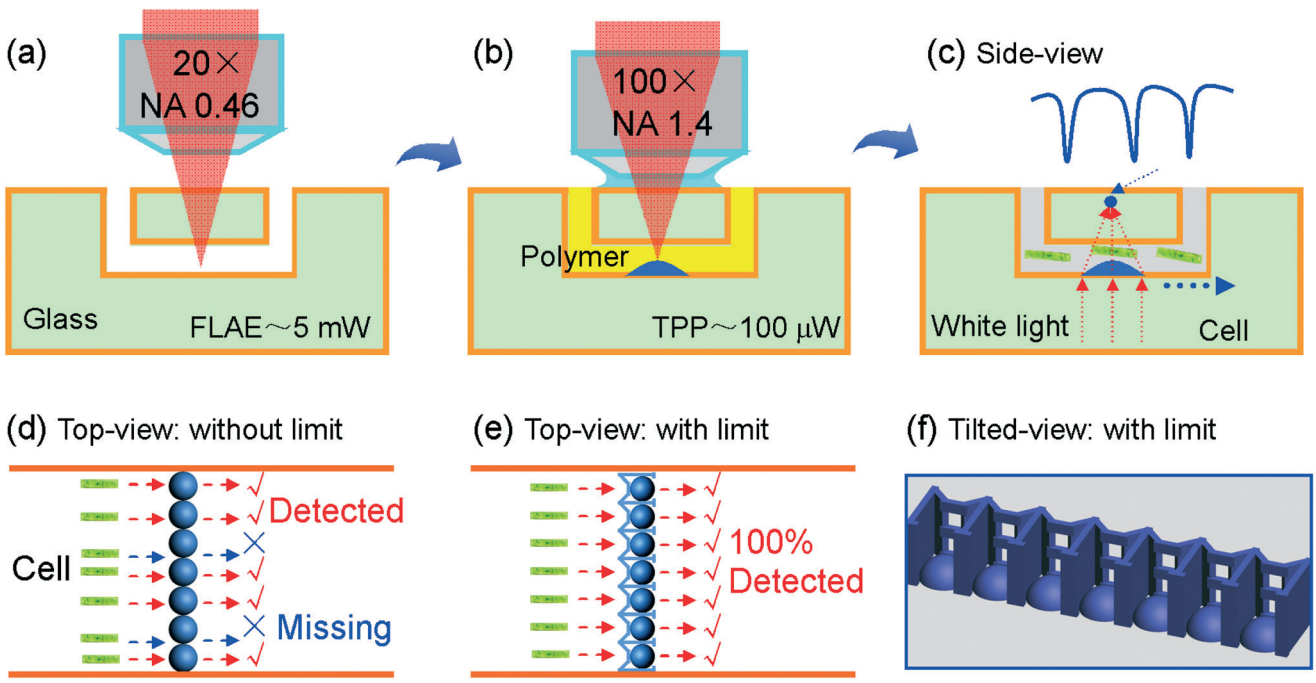

Fig. 1 Fabrication procedure and optimal design for center-pass combined optofluidic MLAs. (a) FLAE for fabrication of a 3D embedded glass microchannel, and (b) TPP for integration of a polymer center-pass MLA. (c) Cell counting by observing the intensity variations at the focal spots of a MLA. When a cell passes across a microlens, it produces an intensity dip. A comparison of (d) a common MLA and (e) a center-pass combined MLA. For the common MLA, cells can pass the border regions between adjacent lenses and escape detection. For a center-pass combined MLA, in contrast, all cells travel above the centers of the microlenses owing to the confining walls and apertures. (f) Tilted view of a center-pass combined MLA having M-shaped confining walls. The apertures control the cells to pass above the center portions of the microlenses.

microchannel. To ensure high performance, flat-scaffold-supported hybrid fs laser microfabrication (FSS-HFLM) is employed. More details of the ship-in-a-bottle integration and FSS-HFLM can be found elsewhere.[32]

In previous experiments, the integrated MLA was used for cell counting by monitoring the intensity variation at the focal spot of each microlens, as illustrated in Fig. 1(c). However, some cells could pass uncounted in the border regions between adjacent lenses, resulting in a reduced 93% success rate, as sketched in Fig. 1(d). To realize 100% cell detection, the center-pass confining wall indicated in Fig. 1(e) forces all cells to pass through the space above the center of each microlens. The schematic in Fig. 1(f) shows a confining wall with apertures that open toward the center of each lens. The cells pass through the apertures and are guided to the spaces above the centers.

Characterization of a 3D glass microchannel with integrated central-pass combined MLAs

A home-made pump-assisted cell counting system (sketched in the ESI† Fig. S1) characterizes the optical functionality of the 3D integrated microchips and demonstrates coupling-free parallel cell counting. The system consists of a halogen lamp, a CCD, and a 50× objective lens. Under white-light illumination from a halogen lamp, the focal spots produced by the MLA are collected by the objective lens and CCD. To measure the focal length of MLA, the objective lens was first used to observe the position of the MLA. Then, the objective lens was moved to see the position of the focal spots of MLA. The distance between these two positions corresponds to the focal length of MLA. Solvents containing cells are introduced into the biochip by a pump. The flow speed can be controlled from 0 to 5 mm s^{-1}. The halogen lamp, CCD, and objective

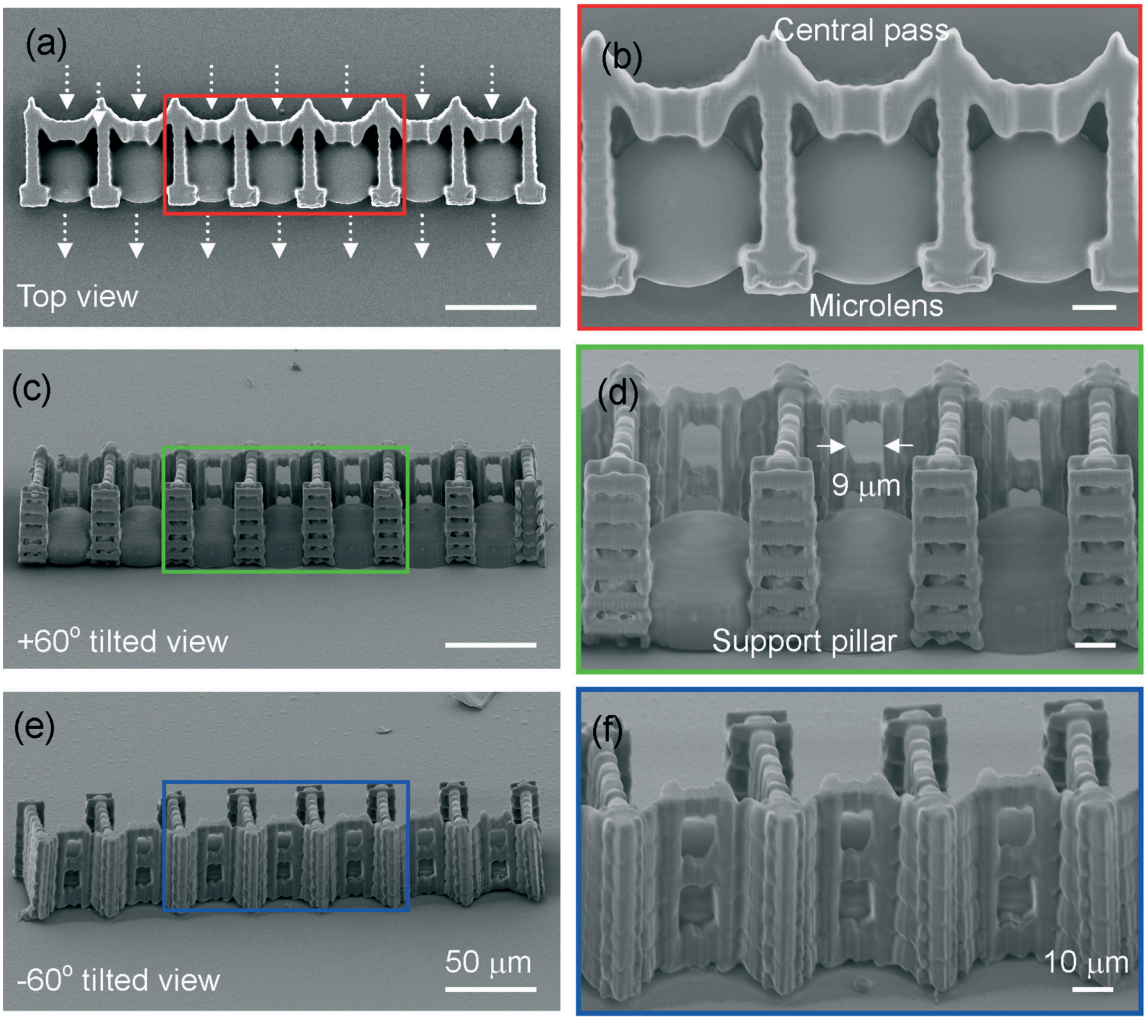

Fig. 2 TPP fabrication of a center-pass combined MLA on a flat glass surface. (a) Top view and (b) magnified (of the red portion) SEM images of a center-pass combined MLA fabricated by TPP. A small pitch of 200 nm is used in laser scanning to realize smooth surfaces. (c) 60° tilted and (d) magnified (of the green portion) SEM images. The aperture size is 9 μm, slightly bigger than the 6–8 μm cells used for counting. 15 μm-width support pillars were fabricated to keep the device constructed after the developing process in TPP. The multilayer web shape provides stability and decreases the fabrication time. (e) 60° tilted and (f) magnified (of the blue portion) SEM images observed from another direction. The confining wall is fabricated with a larger scanning pitch of 800 nm to decrease the total fabrication time to 1.8 h.

lens allow simultaneous *in situ* monitoring of the temporal intensity variation of each focal spot.

3. Results and discussion

Optimal design and fabrication of a center-pass combined MLA on a flat glass surface

To optimize the design of the polymer microcomponents and TPP experimental parameters, a center-pass combined MLA is first fabricated on a flat glass surface. Fig. 2(a) and (b) exhibit top-view SEM images of the center-pass combined MLA having a 280 μm width and containing seven microlenses and an M-shaped confining wall. The lens diameter and height are 34 and 6 μm, respectively. For integration of this device inside a microfluidic channel, a flat scaffold is constructed to eliminate the influence of the undulated bottom surface of the microchannel described previously.[32] Specifically, a 5 μm flat scaffold is fabricated. Each M-shaped wall has two apertures, as seen in the 60°-tilted SEM images in Fig. 2(c)–(f). The wall thickness is 6 μm, as shown in Fig. 3(a) and (b), and the aperture is 9 μm × 9 μm, as seen in Fig. 2(c) and (d), which is 2 μm bigger than the average size (~7 μm) of counted cells. The aperture size should be designed by the kind of targeted cell and be slightly bigger than the cell size. Bigger or smaller aperture size can be designed using a computer program, and then be easily fabricated by fs-laser TPP since this technique has excellent flexibility due to its point-to-point scanning strategy. For fabrication of the bigger aperture to count larger cells, *e.g.*, some kinds of mammalian cells, there is in principle no limitation in fabrication. Meanwhile, the processing resolution (~100 nm) of our technique limits the fabrication of smaller apertures to several hundred nanometers.[26] The height of walls is 40 μm, so that the walls fabricated at a laser power of 50 μW are easily deformed due to relatively thin wall thickness, as shown in the ESI† Fig. S2. To avoid such deformations, a higher laser power of 70 μW is used to produce a thicker wall of 8 μm. In addition, 15 μm-wide pillars are fabricated

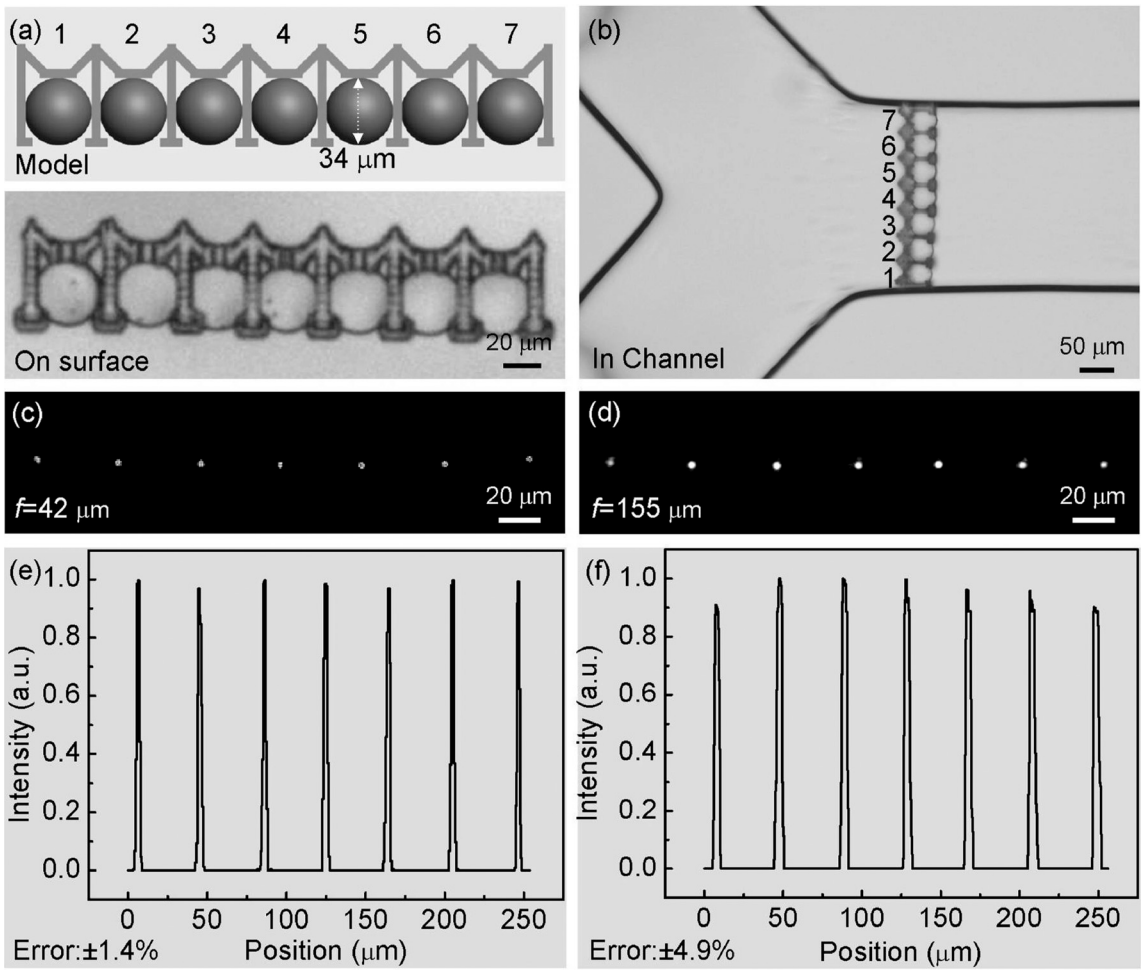

Fig. 3 Integration of a center-pass combined MLA into a 3D embedded glass microchannel. (a) Schematic and (b) microscopic images of the devices on a flat surface and in a closed microchannel. Focusing characteristics of center-pass combined MLAs (c) on a surface and (d) in a channel. The measured focal length on the flat surface is 42 ± 3 μm in air (with n_{air} = 1), and it is 155 ± 5 μm in a channel filled with ethanol (for which $n_{ethanol}$ = 1.362). These agree with the theoretical values of 39.8 μm in air and 159.6 μm in ethanol from the ESI† Fig. S3. Intensity of the focal spots of the MLAs with variations (e) on a flat surface of ±1.4% and (f) of ±4.9% in a channel is due to the influence of the channel sidewalls.

to support the device during the solvent development process. These support pillars are designed as a multilayer web shape, which provides stability and decreases the fabrication time. To further decrease the fabrication time to 1.8 h, a larger scanning pitch of 800 nm is adopted for the confining wall structure. As shown in Fig. 2(e) and (f), the wall surface is a bit rough due to the larger scanning pitch, but that does not affect the operation of the device. On the other hand, for the microlens fabrication, a scanning pitch of 200 nm is used to produce smooth surfaces, as shown in Fig. 2(b), to ensure high performance.

Integration and characterization of a center-pass combined MLA in glass microchannels

A similar device is integrated into a 3D closed glass microchannel. As shown in the microscopic image in Fig. 3(b), the M-shaped confining walls and seven microlenses realized under the optimal laser power of 140 μW exhibit no visible deformations. The ship-in-a-bottle integration usually requires higher laser power as compared with the fabrication on a glass surface, due to reflection and scattering at the channel/polymer interface as well as multiphoton absorption in the glass and polymer.[26] Under white-light illumination, both the center-pass combined MLAs on the surface and in the channel produce bright focal spots. The measured focal length on the flat surface is 42 ± 3 μm in air (n_{air} = 1), while that in a channel filled with ethanol (for which $n_{ethanol}$ = 1.362) is 155 ± 5 μm. These agree well with the theory according to the aplanatic principle and refractive formula illustrated in the ESI† Fig. S3. In air the focal length is

$$f = \frac{r^2 + h^2 - h^2 n_{su8}{}^2}{2h(n_{su8} - 1)} + h = 39.8\ \mu\text{m}, \quad (1)$$

where r and h are the radius and height of the microlens, respectively. In ethanol, the theoretical focal length of the microlens is 159.6 μm, which is much longer than that in air owing to the smaller difference in the refractive indices of the polymer (n_{su8} = 1.58) and ethanol compared to the

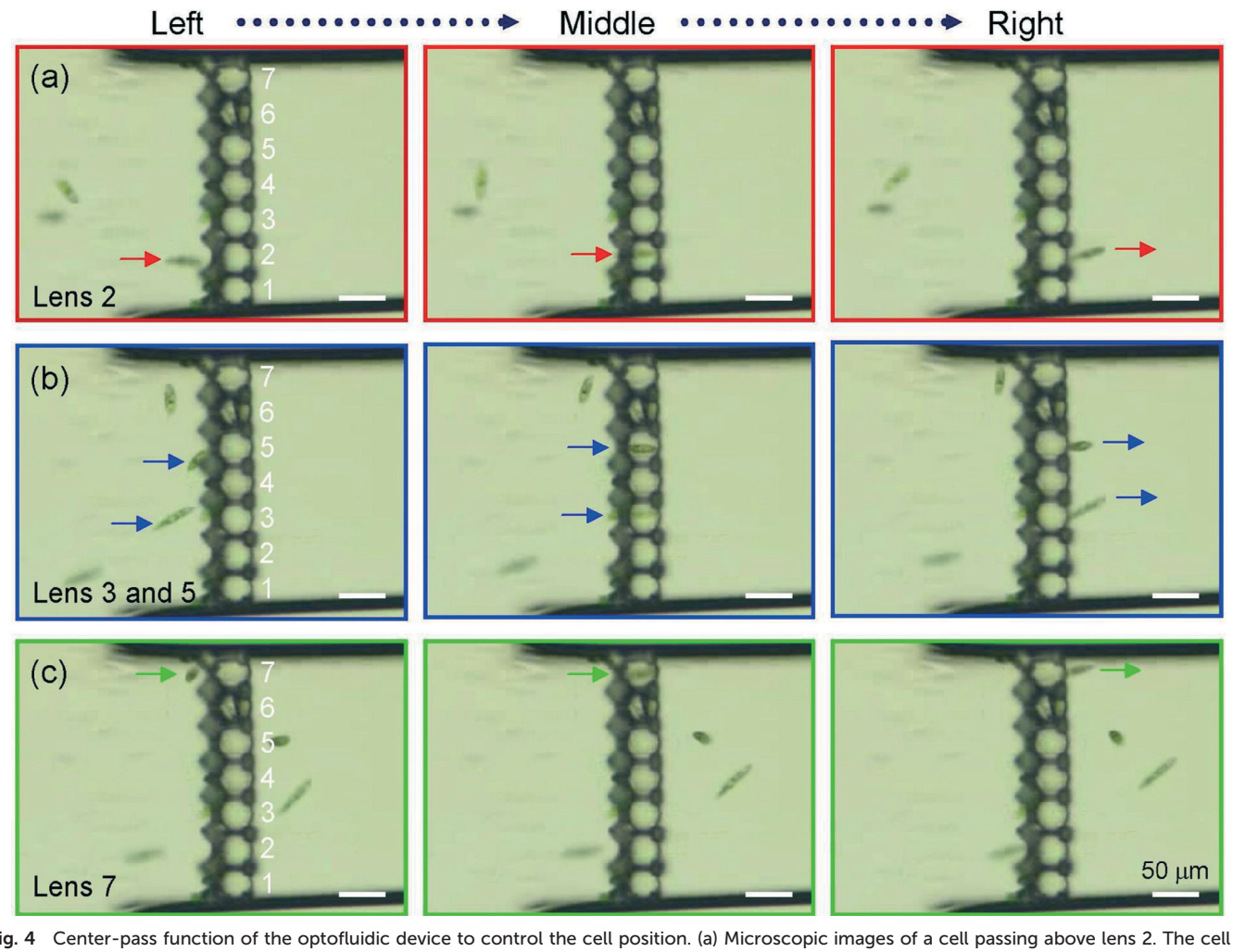

Fig. 4 Center-pass function of the optofluidic device to control the cell position. (a) Microscopic images of a cell passing above lens 2. The cell is initially located on the left side of the device in the microchannel. Then it passes through the aperture in the confining wall above the center part of the lens. Finally it reaches the right side of the device. (b) and (c) Three cells pass above the centers of microlenses 3, 5, and 7 from left to right.

polymer and air. The uniformity of the intensity at each focal spot in the array is investigated by extracting the grayscale intensity from the microscopic images in Fig. 3(c) and (d), as summarized in the ESI† Tables S1 and S2. The deviation in the intensity on a flat surface is ±1.4%, as shown in Fig. 3(e), whereas that in a channel is ±4.9%, as indicated in Fig. 3(f) and the ESI† Table S1. Due to the influence of the channel sidewalls, the optical intensity of the focal spots adjacent to the sidewalls is slightly lower than elsewhere, as we expected, which causes the higher deviation.

The center-pass function of the optofluidic device to control cell positions

The ability to control the cells so that they pass through the space above the center of a microlens is a key to ensuring 100% cell detection. To systemically investigate this center-pass function, several cells were introduced into a microfluidic channel filled with water. Shown in Fig. 4(a) is a microscopic image of a cell passing above the second lens from the left. The living cells used for counting are *Euglena gracilis*, which is a flagellated laboratory microorganism living in freshwater environments and represents one of the simplest and earliest derived eukaryotic cells.[40] The size of this cell ranges between 50 μm and 80 μm length and 6 μm and 12 μm width, depending on cell age and culture conditions. The average width of cells used in this study was 7 μm ranging from 6 μm to 8 μm. First the cell is on the left side of the device in the microchannel. Then it passes through the aperture in the confining wall. Next it crosses the center of the microlens from left to right. Finally it reaches the right side of the device. Similarly, as seen in Fig. 4(b) and (c), three cells pass above the center parts of microlenses 3, 5, and 7. Interestingly, two cells are passing above different microlenses at nearly the same time in Fig. 4(b), demonstrating the possibility to simultaneously detect multiple cells for parallel counting. The ESI†

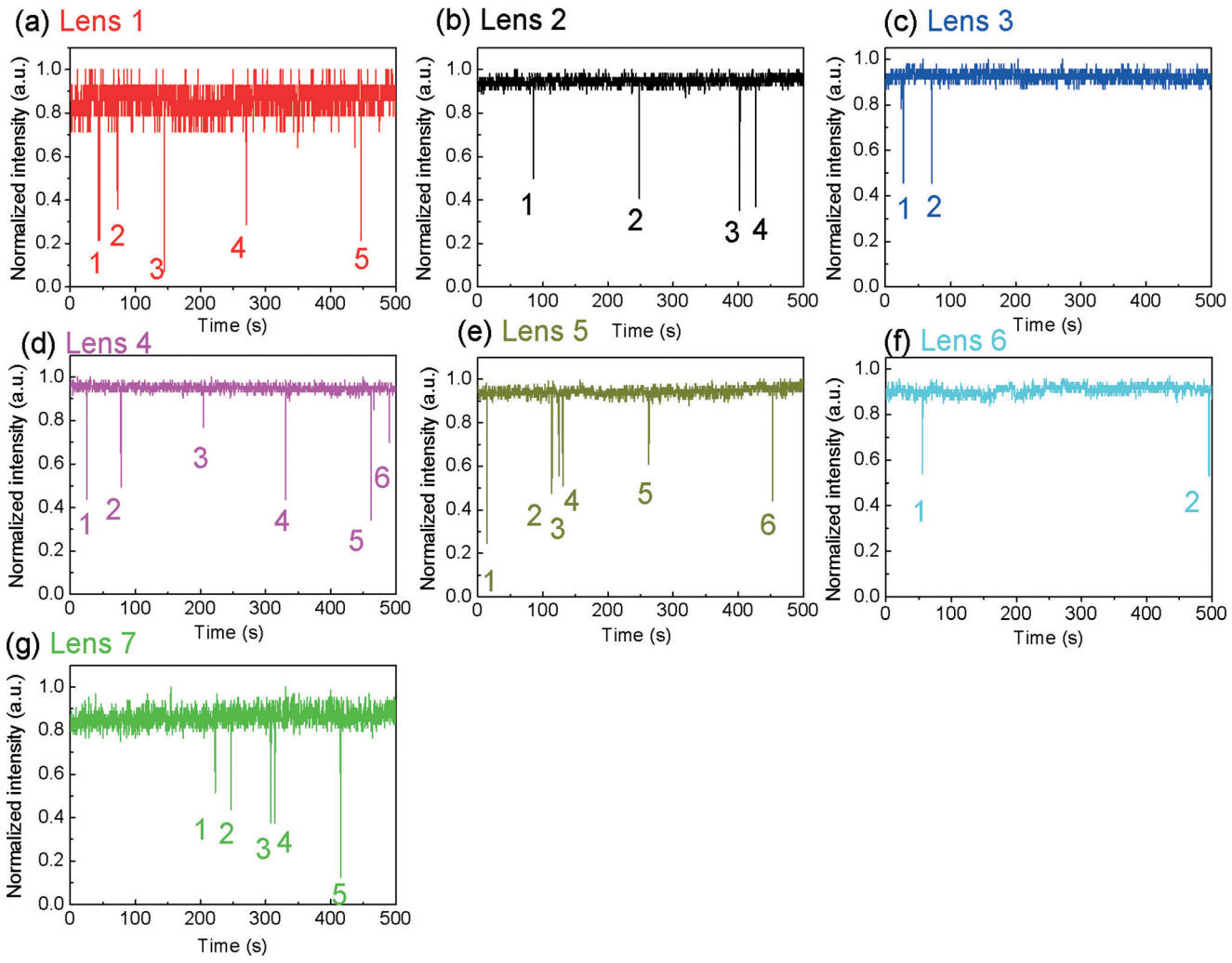

Fig. 5 Demonstration of 100% cell counting by a center-pass combined optofluidic MLA. Time-dependent variations in the intensity at the focal spots of seven microlenses in an array. When thirty cells are placed into the channel at a flow speed of 50–100 μm s^{-1}, thirty intensity dips are obtained. Each intensity dip corresponds to one cell passing above a microlens. This demonstrated that all cells were detected by the center-pass combined optofluidic MLA (100% success rate) and no cells were missed.

Video S1 further verifies that the apertures in the confining wall can control every cell so that they pass above the centers of the microlenses.

Demonstration of the 100% success rate for cell counting by a center-pass combined optofluidic MLA

The microlenses can produce bright focal spots under white-light illumination. However, once a cell passes above the center of a microlens, the intensity of the focal spot significantly decreases because the cell scatters, reflects, and absorbs the incident light.[32] By monitoring the focal spots of seven lenses, the intensity is observed to vary with time, as graphed in Fig. 5. Every intensity dip corresponds to one cell passing above a microlens. When 30 cells are placed in a water-filled channel, 30 intensity dips are obtained. This result demonstrates that all cells are detected by the center-pass combined optofluidic MLA, in contrast to previous work in which about 7% of the cells passed through the edge regions between adjacent lenses and were not detected. The flow speed of

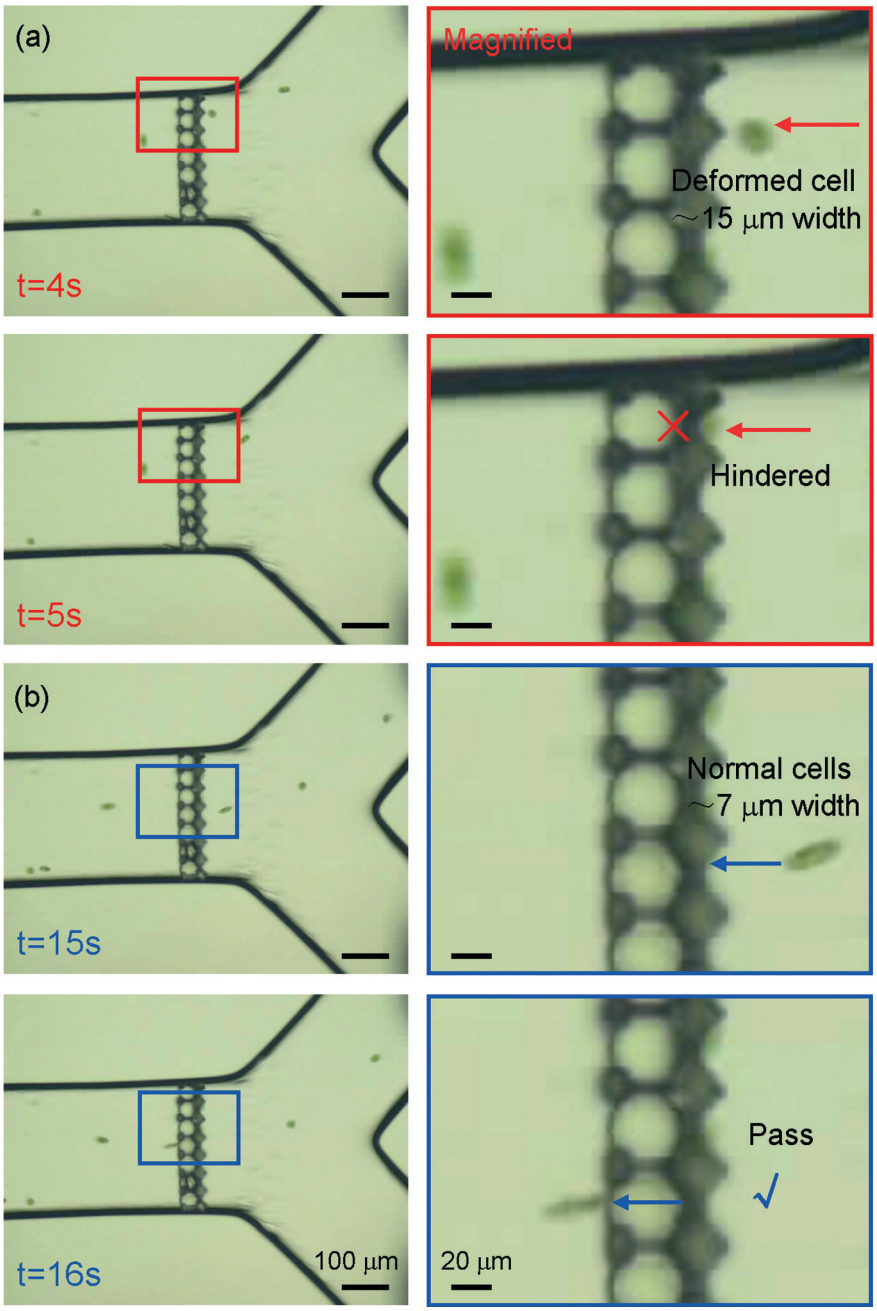

Fig. 6 Filtering of deformed cells by a center-pass combined optofluidic MLA. (a) Some cells have a round shape due to biological deformation. The diameter of such cells can be as large as 15 μm. They are hindered from passing by the 9 μm apertures in the confining wall. (b) Normal cells with 6–8 μm width can freely pass the apertures in the wall. Also see the ESI† Video 2.

50–100 μm s^{-1} employed in this study enables us to clearly count the cell number by observation using an optical microscope and compare with the number of intensity dips. For practical use of this system, the higher flow rate commonly used in microfluidic channels (1–10 mm s^{-1}) is applicable by adoption of a rapid response CCD. The cell concentration was chosen to be 10^2–10^6 ml^{-1}, since a higher concentration makes it difficult to secern the two adjacent cells due to their too close distance. The ability to control the cell position in a microchip is also important for other types of cell detection and manipulation.[17–19,29–31] To control cell positions, various strategies have previously been developed such as decreasing the neck size of the microchannels to match the targeted cell size,[29–31] fabricating small-size parallel sub-channels,[41] using flow electrokinetic[17,18] or hydrodynamic focusing,[19] which usually lead to complex process or difficult operation. The center-pass combined microlens arrays are designed with a computer and fabricated by single-step laser scanning, so that the fabrication of complex structures does not increase difficulty in the experiment. Additionally, the center-pass unit has an additional function of cell filtering as described below, which enables us to count specific size of cells. The intensity dips show some variations, which may be caused by three factors. First, the apertures are slightly larger than the cells. This causes small variations in the cell positions above the microlenses, as seen in the ESI† Fig. S4. Second, the cells can pass a microlens at different heights in the microchannel mostly due to two apertures formed at the different height in the center pass unit. If the cells pass the aperture at the lower position, the intensity dips will be bigger, while at the upper position, will be smaller. Third, the cell sizes are not all identical but range from 50 × 6 μm to 72 × 8 μm (length × width). These variations do not affect the performance of the center-pass combined optofluidic MLA in terms of easy operation, high success rate (100%) and parallel detection. To count different kinds of cells, the aperture size should be designed to be slightly larger than the size of targeted cells. Thus, any cells can be directed to almost the center part of the microlens, resulting in a 100% success rate in counting. In this demonstration, only 30 cells were introduced into the channel. This optofluidic system can handle the larger number and higher density of cells as far as the sizes of all cells introduced are smaller than the aperture size. However, the samples containing cells larger than the aperture size may cause clogging of the apertures. To minimize the possibility of clogging, the center-pass unit was designed to have two apertures.

Finally, the ability of a center-pass combined optofluidic MLA to filter deformed cells is demonstrated in Fig. 6. Some cells are rounded because of biological deformation. Their size can be as large as 15 μm, so that they are hindered by the 9 μm aperture, in contrast to normal cells of 6–8 μm width. The ESI† Video 2 shows more details. The flow speed is not uniform across the microchannel, *i.e.*, the flow speed at the center of the channel is faster than that at the edge of the channel. But this may not affect the filtering ability of the aperture, which is mainly determined by the relative sizes between the aperture and the cell.

4. Conclusion

A novel cell-counting device is proposed: a center-pass combined optofluidic MLA having confining walls with 9 μm apertures. By optimizing the TPP experimental parameters, the polymer devices can be successfully integrated into a closed glass microchannel. The microlens arrays produce multiple focal spots with a uniform optical intensity (within ±5%) under white-light illumination. The confining walls and apertures permit only cells of 6–8 μm width to pass above adjacent microlenses. As cells cross that space, the intensity of the focal spots decreases due to optical scattering, reflection, and absorption by the cells. By monitoring the time-dependent optical intensity variations at each focal spot, coupling-free parallel cell counting with a 100% success rate is enabled. Additionally, the apertures not only control the position of each cell but they can also filter out deformed cells of 15 μm width. Such high-performance cell-counting devices will greatly enhance the functions of LOC systems and offer broad applications in biological cell analysis, medical diagnostics,[42] and cell manipulations owing to their simple operation, high success rate of detection, and parallel sensing.[43,44] Furthermore, this kind of optofluidics will be applicable to identify different kinds of cells by detecting fluorescence signals.

Acknowledgements

This work was supported by JSPS KAKENHI grant number 25286038. The authors thank Prof. Atsushi Miyawaki and Dr. Hiroyuki Kawano from the Laboratory for Cell Functions and Dynamics at the Brain Science Institute of RIKEN for useful discussions and technical assistance.

References

1 M. W. Losey, M. A. Schmidt and K. F. Jensen, *Ind. Eng. Chem. Res.*, 2001, **40**, 2555–2562.
2 M. A. Burns, B. N. Johnson, S. N. Brahmasandra, K. Handique, J. R. Webster, M. Krishnan, T. S. Sammarco, P. M. Man, D. Jones, D. Heldsinger, C. H. Mastrangelo and D. T. Burke, *Science*, 1998, **282**, 484–487.
3 L. Y. Yeo, H. C. Chang, P. P. Y. Chan and J. R. Friend, *Small*, 2011, **7**, 12–48.
4 D. Psaltis, S. R. Quake and C. Yang, *Nature*, 2006, **442**, 381–386.
5 X. Fan and I. M. White, *Nat. Photonics*, 2011, **5**, 591–597.
6 H. Schmidt and A. R. Hawkins, *Nat. Photonics*, 2011, **5**, 598–604.
7 T. McCreedy, *TrAC, Trends Anal. Chem.*, 2000, **19**, 396–401.
8 D. C. Duffy, J. C. McDonald, J. A. Schueller and G. M. Whitesides, *Anal. Chem.*, 1998, **70**, 4974–4984.
9 D. Qin, Y. Xia and G. M. Whitesides, *Nat. Protoc.*, 2010, **5**, 491–502.
10 E. A. Ottesen, J. W. Hong, S. R. Quake and J. R. Leadbetter, *Science*, 2006, **314**, 1464–1467.

11 L. Martin, M. Meier, S. M. Lyons, R. V. Sit, W. F. Marzluff, S. R. Quake and H. Y. Chang, *Nat. Methods*, 2012, **9**, 1192–1194.
12 D. A. Dunn and I. Feygin, *Drug Discovery Today*, 2000, **5**, S84–S91.
13 H. Craighead, *Nature*, 2006, **442**, 387–393.
14 M. J. Fulwyler, *Science*, 1965, **150**, 910–911.
15 J. A. Steinkamp, *Rev. Sci. Instrum.*, 1984, **55**, 1375–1400.
16 P. Friis, K. Hoppe, O. Leistiko, K. B. Mogensen, J. Hubner and J. P. Kutter, *Appl. Opt.*, 2001, **40**, 6246–6251.
17 L. M. Fu, R. J. Yang, C. H. Lin, Y. J. Pan and G. B. Lee, *Anal. Chim. Acta*, 2004, **507**, 163–169.
18 C. H. Lin and G. B. Lee, *J. Micromech. Microeng.*, 2003, **13**, 447–453.
19 Z. Wang, J. El-Ali, M. Engelund, T. Gotsaed, I. R. Perch-Nielsen, K. B. Mogensen, D. Snakenborg, J. P. Kutter and A. Wolff, *Lab Chip*, 2004, **4**, 372–377.
20 J. Wang, Y. He, H. Xia, L. G. Niu, R. Zhang, Q. D. Chen, Y. L. Zhang, Y. F. Li, S. J. Zeng, J. H. Qin, B. C. Lin and H. B. Sun, *Lab Chip*, 2010, **10**, 1993–1996.
21 M. H. Olsen, G. M. Hjorto, M. Hansen, O. Met, I. M. Svane and N. B. Larsen, *Lab Chip*, 2013, **13**, 4800–4809.
22 T. W. Lim, Y. Son, Y. J. Jeong, D. Y. Yang, H. J. Kong, K. S. Lee and D. P. Kim, *Lab Chip*, 2011, **11**, 100–103.
23 Y. He, B. L. Huang, D. X. Lu, J. Zhao, B. B. Xu, R. Zhang, X. F. Lin, Q. D. Chen, J. Wang, Y. L. Zhang and H. B. Sun, *Lab Chip*, 2012, **12**, 3866–3869.
24 L. Amato, Y. Gu, N. Bellini, S. M. Eaton, G. Cerullo and R. Osellame, *Lab Chip*, 2012, **12**, 1135–1142.
25 R. Osellame, H. J. W. M. Hoekstra, G. Cerullo and M. Pollnau, *Laser Photonics Rev.*, 2011, **5**, 442–463.
26 D. Wu, S. Z. Wu, J. Xu, L. G. Niu, K. Midorikawa and K. Sugioka, *Laser Photonics Rev.*, 2014, **8**, 458–467.
27 K. Sugioka and Y. Cheng, *Appl. Phys. A: Mater. Sci. Process.*, 2014, **114**, 215–221.
28 K. Sugioka, J. Xu, D. Wu, Y. Hanada, Z. Wang, Y. Cheng and K. Midorikawa, *Lab Chip*, 2014, **14**, 3447–3458.
29 M. Kim, D. J. Hwang, H. Jeon, K. Hiromatsu and C. P. Grigoropoulos, *Lab Chip*, 2009, **9**, 311–318.
30 A. Schaap, T. Rohrlack and Y. Bellouard, *Lab Chip*, 2012, **12**, 1527–1532.
31 R. Osellame, V. Maselli, R. M. Vazquez, R. Ramponi and G. Cerullo, *Appl. Phys. Lett.*, 2007, **90**, 231118.
32 D. Wu, J. Xu, L. G. Niu, S. Z. Wu, K. Midorikawa and K. Sugioka, *Light: Sci. Appl.*, 2015, **4**, e228.
33 S. Kawata, H. B. Sun, T. Tanaka and K. Takada, *Nature*, 2001, **412**, 697–698.
34 S. Maruo, O. Nakamura and S. Kawata, *Opt. Lett.*, 1997, **22**, 132–134.
35 L. Li, R. R. Gattass, E. Gershgoren, H. Hwang and J. T. Fourkas, *Science*, 2009, **324**, 910–913.
36 Z. Gan, Y. Cao, R. A. Evans and M. Gu, *Nat. Commun.*, 2013, **4**, 2061.
37 A. Ledermann, L. Cademartiri, M. Hermatschweiler, C. Toninelli, G. A. Ozin, D. S. Wiersma, M. Wengener and G. V. Freymann, *Nat. Mater.*, 2006, **5**, 942–945.
38 W. Xiong, Y. S. Zhou, X. N. He, Y. Gao, M. M. Samani, L. Jiang, T. Baldacchini and Y. F. Lu, *Light: Sci. Appl.*, 2012, **1**, e6.
39 K. Sugioka, Y. Hanada and K. Midorikawa, *Laser Photonics Rev.*, 2010, **3**, 386–400.
40 M. Iseki, S. Matsunaga, A. Murakami, K. Ohno and K. Shiga, *Nature*, 2002, **415**, 1047–1051.
41 E. Schonbrun, A. R. Abate, P. E. Steinvurzel, D. A. Weitz and K. B. Crozier, *Lab Chip*, 2010, **10**, 852–856.
42 Y. Wu, D. Xing, L. Liu, T. Chen and W. R. Chen, *Acta Biochim. Biophys. Sin.*, 2007, **39**, 37–45.
43 D. G. Grier, *Nature*, 2003, **424**, 810–816.
44 N. Bellini, K. C. Vishnubhatla, F. Bragheri, L. Ferrara, P. Minzioni, R. Ramponi, I. Cristiani and R. Osellame, *Opt. Express*, 2010, **18**, 4679–4688.